Applied Catalysis B: Environmental 221 (2018) 584–597

Contents lists available at ScienceDirect

Applied Catalysis B: Environmental

journal homepage: www.elsevier.com/locate/apcatb

Research paper

Co-production of hydrogen and carbon nanotubes from real-world waste plastics: Influence of catalyst composition and operational parameters

Dingding Yao[a,b], Yeshui Zhang[b], Paul T. Williams[b,*], Haiping Yang[a,*], Hanping Chen[a]

[a] State Key Laboratory of Coal Combustion, School of Energy and Power Engineering, Huazhong University of Science and Technology, 430074 Wuhan, China
[b] School of Chemical and Process Engineering, University of Leeds, Leeds, LS2 9JT UK

ARTICLE INFO

Keywords:
Ni-Fe catalyst
Waste
Plastics
Hydrogen
Carbon nanotubes

ABSTRACT

The use of Ni-Fe catalysts for the catalytic pyrolysis of real-world waste plastics to produce hydrogen and high value carbon nanotubes (CNT), and the influence of catalyst composition and support materials has been investigated. Experiments were conducted in a two stage fixed bed reactor, where plastics were pyrolysed in the first stage followed by reaction of the evolved volatiles over the catalyst in the second stage. Different catalyst temperatures (700, 800, 900 °C) and steam to plastic ratios (0, 0.3, 1, 2.6) were explored to optimize the product hydrogen and the yield of carbon nanotubes deposited on the catalyst. The results showed that the growth of carbon nanotubes and hydrogen were highly dependent on the catalyst type and the operational parameters. Fe/γ-Al_2O_3 produced the highest hydrogen yield (22.9 mmol $H_2/g_{plastic}$) and carbon nanotubes yield (195 mg $g^{-1}_{plastic}$) among the monometallic catalysts, followed by Fe/α-Al_2O_3, Ni/γ-Al_2O_3 and Ni/α-Al_2O_3. The bimetallic Ni-Fe catalyst showed higher catalytic activity in relation to H_2 yield than the monometallic Ni or Fe catalysts because of the optimum interaction between metal and support. Further investigation of the influence of steam input and catalyst temperature on product yields found that the optimum simultaneous production of CNTs (287 mg $g^{-1}_{plastic}$) and hydrogen production (31.8 mmol $H_2/g_{plastic}$) were obtained at 800 °C in the absence of steam and in the presence of the bimetallic Ni-Fe/γ-Al_2O_3 catalyst.

1. Introduction

The worldwide demand for plastics grows rapidly and inevitably produces large quantities of waste plastics. Over 60% of post-consumer plastics ends up in waste landfills or is incinerated, representing a waste of resource [1]. Thermal recycling via pyrolysis and gasification of waste plastics, into fuels and chemical products has been identified as a promising technology for tackling waste issues related to plastics [2,3]. In recent years, an attractive method of producing high value nanomaterials such as carbon nanotubes (CNTs) from waste plastics has been reported [4,5]. The produced CNTs were further utilised to produce reinforced materials which exhibited improved strength characteristics, implying the potential of the process in industrial applications [6].

Due to their extraordinary properties including chemical stability, electric conductivity, high surface area, etc., carbon nanotubes have been attracting worldwide attention [7–9]. Compared with other synthesis technologies which include arc discharge and laser ablation, chemical vapour deposition (CVD) is the most prevalent and versatile technology in terms of cost and bulk production. Research into CVD for CNT production has been reported to convert methane, ethylene, ethanol to carbon nanotubes through CVD [10,11]. Thermal conversion of plastics to carbon nanotubes can be achieved in two stage reactors, where solid plastics are pyrolysed to produce volatile materials in a first stage (temperature around 500 °C), followed by CVD at high temperature over a catalyst [12,13]. Hydrogen, which will be an important clean fuel in the future, can also be generated during this process.

The hydrogen yield and morphology of the product carbon nanomaterials can be varied with different operational parameters. The growth temperature is a key factor for carbon nanotubes production, as it effects both the hydrocarbon cracking and carbon diffusion rate. A novel fluidized bed reactor was investigated with different temperatures at different stages to obtain a balance between carbon production and diffusion on the catalyst, so that a continuous growth of carbon nanotubes was achieved [14]. Shen et al. [15] used a step-wise heating process for hydrogen and carbon materials production from methane. They reported that bamboo-shaped, multi-branched and onion-like carbons were deposited on the catalyst and their yield varied with increased catalyst temperature. In addition, an increase in catalyst temperature was shown to result in a higher yield of hydrogen from waste plastics [16]. In order to increase the hydrogen yield, steam has often

* Corresponding authors.
E-mail addresses: p.t.williams@leeds.ac.uk (P.T. Williams), yhping2002@163.com (H. Yang).

http://dx.doi.org/10.1016/j.apcatb.2017.09.035
Received 6 June 2017; Received in revised form 11 September 2017; Accepted 14 September 2017
Available online 18 September 2017

been introduced to promote hydrocarbon reforming reactions which yields more gaseous product. However, as a consequence of steam addition, carbon deposited on the catalyst may also be gasified which leads to a lower carbon yield [17,18]. However, Zhang et al. [19] found that a low level injection of steam could improve the purity of carbon nanotubes without consuming excessive amounts of the carbon.

In addition to the operational parameters, other factors such as feedstock type, external energy (e.g. plasma enhanced) and catalyst to feedstock ratio have also been investigated to optimize the process [20–22]. However, the catalyst composition is considered to be the most influential factor for carbon nanotubes production. It is known that Ni-based catalysts are favorable for thermal conversion of hydrocarbons due to their effective catalytic activity and lower cost. Yang et al. [13] synthesized CNTs with an external diameter of 20–30 nm from polypropylene and polyethylene in a pilot-scale system using a H-Ni/Al_2O_3 catalyst. Wen et al. [23] used a Ni catalyst to form CNTs from polyolefin wastes, which showed good electrochemical performance as electrode material for supercapacitors. Whilst Ni based catalysts are commonly used for hydrogen production, Fe catalysts are more often utilised for carbon nanomaterial production. Acomb et al. [24] investigated the influence of different metal catalysts for the catalytic pyrolysis of low density polyethylene. They reported that an Fe/Al_2O_3 catalyst gave a higher conversion of the hydrogen in the plastic to H_2 gas (26.8% conversion), but also the Fe/Al_2O_3 catalyst produced a high carbon yield on the catalyst (26 wt.%) compared with Ni, Co and Cu based catalysts, due to the high carbon solubility of Fe.

Recently, bimetallic or trimetallic catalysts have received attention to further improve catalyst activity. A porous Ni-Cu-Co alloy catalyst was studied by Lua and Wang [25] for the decomposition of methane for hydrogen and carbon nanotubes production. The interaction between Cu and Fe was found to enhance the nucleation of nanotubes over Fe as well as minimize the bulk accumulation of carbon substrates [26]. In terms of hydrogen production, Wu and Williams [27,28] have suggested that a bimetallic Ni-Mg catalyst presented higher catalytic activity towards hydrogen production than a monometallic Ni catalyst. This was attributed to the reduced amount of monoatomic carbons produced and the enhanced physical stability of the catalyst with the bimetallic catalyst. The advantages of such multi-metal catalysts arises from good stability, smaller metal particle size and appropriate interaction between different metals [29]. Ni-Fe bimetallic catalysts have shown favorable performance for some studies, for example, Ni-Fe based on bio-char has been used in biomass gasification to increase tar conversion in an effective and economical way [30]. Enhanced methane dehydrogenation and longer catalyst life-time activity were found by Shen et al. [31] when using Ni-Fe/Mg(Al)O for CNTs production from methane. However, there are limited reports about using Ni-Fe bimetallic catalysts for the co-production of CNTs and H_2 from waste plastics.

The catalyst substrate is also an important factor for the synthesis of carbon nanotubes. Pure nickel particles without a substrate were found to be a difficult surface to deposit any carbons because of metal agglomeration [32]. The substrate acts not only as a support medium but also a reactant to catalyst and carbon precursors. The physical or chemical interaction between catalyst particles and support can stabilize the metal particles with a finely dispersed particle distribution [10]. As a number of reports in the literature have noted, the diameter of synthesized carbon nanomaterials were closely related to the catalyst metal particle size [33,34]. Thereby, the possibility of controlling the diameter of carbon nanotubes could be achieved. The effect of different catalyst support material properties on carbon nanomaterials production from methane was investigated by Takenaka et al. [35], and showed that Al_2O_3 and MgO supported Co catalysts gave higher carbon yields than Co/TiO_2 and Co/SiO_2. Ermakova et al. [36] reported that the morphology and structure of filamentous carbons on iron catalysts were strongly dependent on the chemical nature of the support.

Although there are a number of studies that have described the use of Fe or Ni based catalysts to catalyse the pyrolysis of hydrocarbons for carbon nanotubes production, most of them focus on small-molecule sized feedstock or single pure polymers. Available studies on Ni-Fe catalysts for the pyrolysis of real world waste plastics are quite limited. Moreover, the hydrogen yield and properties of carbon deposits using Ni-Fe with different supports, catalyst temperature and steam injection have not been systematically investigated. Therefore, this paper aims to explore monometallic Ni, Fe and bimetallic Ni-Fe catalysts for the pyrolysis of waste plastics. The effect of catalyst composition and substrate type on the yield and morphology of deposited carbon, as well as the hydrogen yield have been investigated. In addition, catalytic reforming of waste plastics under different catalyst temperatures and steam to plastic ratios were conducted to further optimize the process.

2. Materials and methods

2.1. Materials

Real-world waste plastics, including disposable drink cups, lunch boxes and plastic wraps, which are widely used for food packing, were collected and used for the process feedstock and were obtained from Mingjin Plastic Ltd, China. The plastic waste was crushed and ground using a liquid nitrogen grinder with screen meshsize between 0.1 and 1 mm. The mixed plastic waste composition was comprised of 40 wt.% sample bottles (mainly HDPE), 35 wt.% plastic bags (mainly LDPE), 20 wt.% preservative boxes (mainly PP) and 5 wt.% lunch boxes (mainly PS). The ultimate analysis of the material was 84.51 wt.% carbon, 13.85 wt.% hydrogen, 1.51 wt.% oxygen and 0.13 wt.% sulphur. Ash content of the mixed plastics was less than 1 wt.%.

Monometallic Ni or Fe based catalyst and bimetallic Ni-Fe catalyst were prepared using an impregnation method. Metal nitrates and two different crystalline forms of alumina (α-Al_2O_3 and γ-Al_2O_3, supplied by Sigma Aldrich, UK) were used as the support material. Both alumina forms are resistant to high temperature and are considered to be stable catalyst supports. Ni/α-Al_2O_3 was prepared starting with 5.503 g of Ni$(NO_3)_3{\cdot}6H_2O$ dissolved in ethanol, followed by addition of 10 g α-Al_2O_3, so that the initial metal loading was 10 wt.%. The precursors were stirred for 4 h using a magnetic stirrer and dried at 50 °C overnight to remove the remaining ethanol. The solid was then calcined at 800 °C with a heating rate of 10 °C min^{-1} and a hold time at 800 °C of 3 h under an air atmosphere. The other catalysts Ni/γ-Al_2O_3, Fe/α-Al_2O_3, Fe/γ-Al_2O_3 and Ni-Fe/γ-Al_2O_3 were synthesized using the same procedure. Bimetallic Ni-Fe catalyst was prepared with the same 10 wt.% of total metal loading but with a Ni to Fe molar ratio of 1–3, which was the optimum composition for the highest yield of carbon depositions and hydrogen yield in preliminary studies [37]. All the catalysts were then crushed and sieved to give granules in the size range of 0.05–0.18 mm. No reduction of the catalyst prior to the catalytic pyrolysis was carried out as the gases produced during pyrolysis-catalytic process such as H_2 and CO reduced the metal oxides in situ.

2.2. Experimental setup and procedure

The pyrolysis-catalysis of waste plastics was conducted in a two-stage fixed bed reactor as shown in Fig. 1. The experimental system consisted of a quartz tube reactor (I.D. 40 mm) with two temperature ranges (upper: pyrolysis zone, 310 mm height; lower: catalysis zone, 310 mm height), a gas supply system, gaseous product condensing system with ice and water mixture and a gas cleaning system followed by an off-line gas product, gas analysis system.

Three sets of experiment were carried out to determine the influence of process parameters on the production of hydrogen and carbon nanotubes; the effect of different catalyst type using Ni/γ-Al_2O_3, Ni/α-Al_2O_3, Fe/γ-Al_2O_3, Fe/α-Al_2O_3 and Ni-Fe/γ-Al_2O_3 catalysts; the influence of steam to plastic mass ratios of 0, 0.3, 1, 2.6; and catalytic temperatures of 700, 800, 900 °C. For each experiment, 0.5 g catalyst

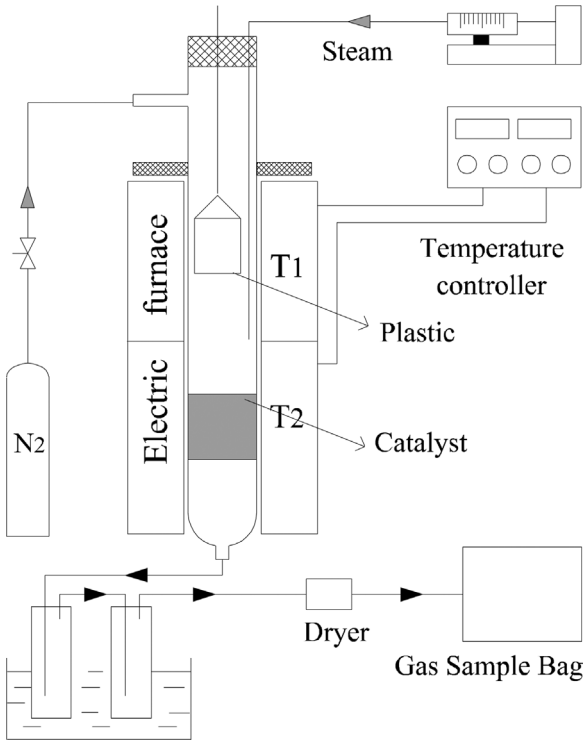

Fig. 1. Schematic diagram of the pyrolysis-catalysis process of waste plastics.

was supported by ~0.2 g stainless steel wire mesh on a perforated plate, which was placed in the middle of the second catalytic stage, where the temperature was preheated to 800 °C. A quartz boat with 1 g of waste plastic was held in the first reactor. High purity nitrogen (99.99%) was supplied as an inert gas at a flow rate of 110 ml min^{-1}. After the second catalyst reactor reached the pre-set temperature and was stable, the boat containing the plastic sample was introduced into the middle of the first stage pyrolysis reactor. The plastic was heated at a controlled heating rate of 10 °C min^{-1} from room temperature to 500 °C and held at 500 °C for 15 min. The condensable product vapours were collected by a two-stage ice-water condenser. The non-condensable gas stream was collected with a 20 l gas sample bag. Gas composition was determined using a dual-channel gas chromatograph (GC) (Micro-GC 3000A, Agilent Technology, USA) equipped with thermal conductivity detectors. H_2, CO and CH_4 were detected by channel A (molecular sieve 5A column) and CO_2, C_2H_2, C_2H_4, C_2H_6 were measured by channel B (polystyrene chromatographic column). The reproducibility of the reaction system was examined and experiments were repeated to ensure reliability.

2.3. Product characterization and analysis

The fresh Ni or Fe based catalysts were characterized using various analytical techniques. Metal species and crystal structure were determined by X-ray diffraction (XRD, X'Pert PRO, PANalytical B.V., Netherlands), using a scanning step of 0.026° in the 2θ range from 10° to 85°. Peaks were identified using a High Score Plus software package. Temperature programmed reduction (TPR) of the catalysts was undertaken using a Stanton Redcroft TGH1000thermo gravimetric analyzer (TGA). Approximately 30 mg of catalyst sample was preheated to 150 °C at a heating rate of 20 °C min^{-1} and held for 10 min, followed by heating to 900 °C at 10 °C min^{-1} in a reduction atmosphere (5 vol.% H_2/95 vol.% N_2).

The morphologies of deposited carbon on the surface of the catalysts was obtained using a Hitachi SU8230 scanning electron microscope (SEM) operating at 20 kV, and a transmission electron microscope (TEM) using a FEI Tecnai TF20. The thermal stability of the carbon on the catalysts was analysed by temperature-programmed oxidation (TPO) on a Shimadzu TGA. A 10 mg sample of the reacted catalyst was heated from room temperature to 800 °C in air (flow rate, 100 ml min^{-1}) with a heating rate of 15 °C min^{-1} and a hold time of 10 min at 800 °C. Raman spectroscopy of the deposited carbon was carried out to determine the graphitic quality, and the spectrograms were obtained using a LabRAM HR800 (Horiba Jobin Yvon, Japan) Raman spectrometer at a wavelength of 532 nm with Raman shift from 200 to 3500 cm^{-1}.

The mass of each gas was calculated according to the volume content from GC analysis and the flow rate of carrier gas (N_2). The total gas and liquid yield were calculated by gas and liquid mass obtained in relation to the total weight of waste plastics. Carbon deposition yield was determined as the mass difference between fresh and reacted catalyst divided by the mass of feedstock. The mass balance was then obtained based on the sum of gas, liquid and solid yield. For each experiment, less than 0.001 g of residue remained in the first stage after pyrolysis, indicating that the plastics were almost completely converted into vapours, the additives that might exist from the manufacturing process of the plastics were neglected in this work.

3. Results and discussion

3.1. Pyrolysis-catalysis of waste plastics with different catalyst type

3.1.1. Characterization of fresh catalyst

XRD analyses of the different fresh catalysts are shown in Fig. 2. Broad and weak XRD spectral peaks of NiO were observed for the Ni/γ-Al_2O_3 catalyst, while the diffraction peaks of Ni/α-Al_2O_3 were sharp and intense, indicating a highly crystalline nature. Briquet et al. [38] considered the adsorption of Ni clusters on the α-Al_2O_3 surface to be of a very limited extent, the crystal NiO and α-Al_2O_3 can be clearly identified on the surface of the Ni/α-Al_2O_3 catalyst. Similar to the Ni/γ-Al_2O_3 catalyst, the XRD diffraction patterns of Fe/γ-Al_2O_3 showed attenuated and wide features and few peaks indicative of crystalline phases. However, the XRD spectra of the Fe/α-Al_2O_3 catalyst were associated with Fe_2O_3 as well as Al_2O_3. Compared to Ni/γ-$Al_2O_3$and Fe/γ-Al_2O_3, the Ni-Fe/γ-Al_2O_3 catalyst produced moderate and low diffraction intensities. The presence of Fe-Al and Ni-Fe-Al alloy that was observed in the XRD spectra at around 36° with the Ni-Fe/γ-Al_2O_3 catalyst indicated the enhanced interaction between metal and support. The

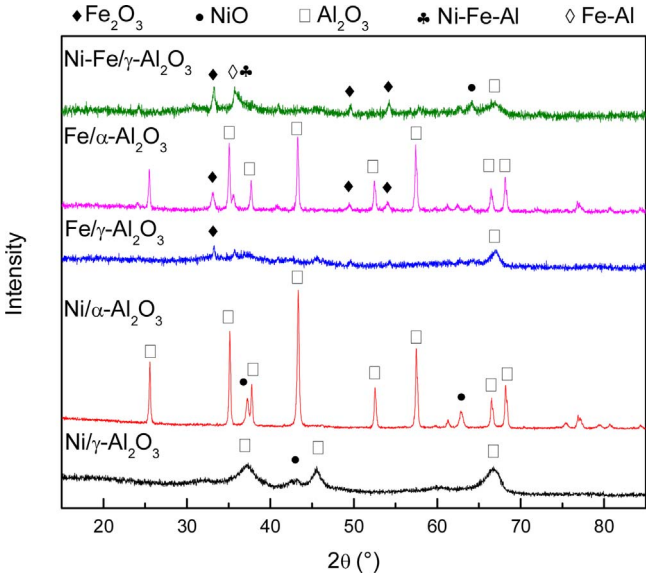

Fig. 2. XRD analysis of fresh Ni and/or Fe based Al_2O_3 catalysts.

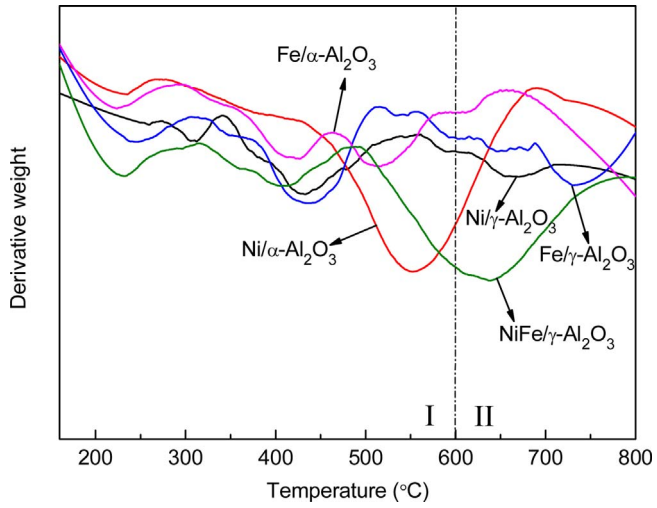

Fig. 3. Temperature programmed reduction of fresh catalysts.

presence of nickel-iron oxide (3, 1, 1) and (2, 2, 2) for the bimetallic Ni-Fe catalysts were also reported by Shen at al. [30] at 35.63 and 37.25° respectively. Similar XRD results for bimetallic catalysts were also observed by Wu and Williams [27,39], where Ni-Mg, Ni-Al and Ca-Al were found from the XRD analysis of fresh catalysts. According to the Scherrer equation, sharp diffraction peaks were linked to higher mean crystallite size and broad peaks related to smaller metal size on the surface of the support [40]. The average crystallite size corresponding to the main phase was calculated as 21, 66, 32, 49 and 20 nm for the Ni/γ-Al_2O_3, Ni/α-Al_2O_3, Fe/γ-Al_2O_3, Fe/α-Al_2O_3 and Ni-Fe/γ-Al_2O_3 catalysts respectively. Therefore, Ni, Fe as well as bimetallic Ni-Fe catalysts remained well dispersed over the γ-Al_2O_3 support. However, metals on the α-Al_2O_3 supported catalysts were agglomerated into larger crystallite sizes, which has also been reported in other literature [41].

The TPR results for the fresh catalysts are displayed in Fig. 3. The Ni/γ-Al_2O_3 catalyst showed two broad peaks at temperatures in the range of 350–500 °C, and at around 650 °C. However, the Ni/α-Al_2O_3 catalyst showed only one reduction peak which occurred at 550 °C. The relatively higher reduction temperature of the Ni/α-Al_2O_3 catalyst compared to that reported by others [42] may be due to the larger particle size (recognized by XRD). The reduction of Fe/γ-Al_2O_3 and Fe/α-Al_2O_3 catalysts are complicated and undergoes a number of stages, which has been reported by other literature [43,44]. It is suggested that Fe_2O_3 is firstly reduced into magnetite at around 400 °C followed by reduction to metallic Fe at higher temperatures, which produces some asymmetric and overlapped peaks. The TPR results of the Ni-Fe/γ-Al_2O_3 catalyst showed a wide range of reductions, including two broad peaks in the range of 300–500 °C and 500–800 °C, respectively.

Alberton et al. [40] observed different reduction profiles for Ni catalysts supported by γ-Al_2O_3 and α-Al_2O_3. Reduction of the Ni/α-Al_2O_3 catalyst was in the range from 300 to 600 °C, whereas it occurred after 600 °C for the Ni/γ-Al_2O_3 catalyst. Fig. 3 shows a division of the catalyst reduction regimes into two temperature regions. It can be seen that all of the catalysts are reduced in the first region (< 600 °C), however, only γ-Al_2O_3 supported catalysts show further reduction at temperatures higher than 600 °C (second region). As derivative peaks at low temperatures are always related to bulk oxides which hardly interact with the support [45], those showing reduction at high temperatures are associated with metal oxides strongly bonded to the alumina support [24]. Therefore, it is suggested that the interaction between Ni (or Fe) with the Al_2O_3 support was stronger in the case of γ-Al_2O_3 compared to α-Al_2O_3. Furthermore, the main TPR reduction peaks found with the Ni/γ-Al_2O_3 and Fe/γ-Al_2O_3 catalysts were in the first region, but changed to the second region in the presence of Ni-Fe/γ-Al_2O_3. The results suggest that the interaction between metal oxides and support was enhanced in the case of bimetallic catalysts compared to monometallic catalysts. In addition, the XRD spectra (Fig. 2) demonstrated the presence of co-spinel-(Ni, Fe, Al) and nickel iron oxide (Fe_2NiO_4 or $FeNi_2O_4$), which were the intermediates that contributed to the interaction between active metals and support. The interaction changes due to the introduction of another metal to a monometallic catalyst have also been reported by other researchers [46,47].

The morphologies and the dispersion of active metallic components of fresh catalysts were determined by SEM-EDX analysis, as shown in Fig. 4. The data shows that the Ni and Fe were well dispersed on the γ-Al_2O_3 support compared to the α-Al_2O_3, which is suggested to be due to the porous nature of the γ-Al_2O_3 support. Both the fresh and externally reduced Ni-Fe/γ-Al_2O_3 catalysts were also characterized using the SEM-EDX (Fig. 4(e) and (f)), little difference in morphologies and metal dispersions between non-reduced and reduced catalyst could be observed, indicating the thermal stability of the prepared Ni-Fe/γ-Al_2O_3 catalyst.

3.1.2. Product yield and gas composition

The influence of different types of catalyst on the yield of products was investigated using the experimental pyrolysis-catalysis system in the absence of any steam input and at a catalyst temperature of 800 °C. The product distribution in terms the yield of gases, liquids and carbon deposition on the catalyst are shown in Table 1. The mass balance for all the catalytic experiments ranged from 95 to 109 wt.%, indicating the reliability of experiments. The only exception was the low mass balance of 80.51 wt.% in the absence of catalyst, which was assigned to the condensed volatiles on the reactor quartz wall, which was difficult to collect and weigh, reducing the reported liquid yield. In addition, the standard deviations of the hydrogen yield and carbon deposition for the repeated experiments were calculated to be in the range of 1.1–1.5 mmol $H_2/g_{plastic}$ and 0.6–1.4 wt.% respectively. It can be seen that the introduction of a catalyst had a significant effect on the hydrogen yield and carbon deposition compared to the non-catalytic experiment (where sand was used for the second stage in place of catalyst). The hydrogen yield and carbon deposition were greatly increased, from 7.9 to 22.5 mmol $H_2/g_{plastic}$ and from 2.2 wt.% to 21.1 wt.% respectively, when the Ni/γ-Al_2O_3 catalyst was used. The Ni/α-Al_2O_3 catalyst generated a lower hydrogen yield (18 mmol $H_2/g_{plastic}$) than the Ni/γ-Al_2O_3 catalyst and was also the lowest yield among the five catalysts. This may due to the undesirable dispersion of Ni particles associated with a large particle size as indicated by XRD results [48]. However, the carbon deposition on Ni/α-Al_2O_3 was 26.1 wt.%, which was significantly higher than over the Ni/γ-Al_2O_3 catalyst. This may be linked to the relatively weak interaction between metal and support which is more likely to increase carbon deposition [17].

The Fe/γ-Al_2O_3 catalyst produced a H_2 yield of 22.9 mmol $H_2/g_{plastic}$ which was higher than the Ni/γ-Al_2O_3 and Ni/α-Al_2O_3 catalysts. As steam was not injected into the reactor system for these experiments, it is suggested that catalytic thermal cracking reactions (Eq.1) which produced carbon deposition and hydrogen were dominant during the process. Therefore, the catalyst with higher yield of carbon deposition also produced a higher hydrogen yield. Therefore, the Fe based catalyst was more active in hydrocarbons cracking and thus showed higher yield of carbon deposition and hydrogen yield than the Ni based catalyst. Previous results reported by Acomb et al. [24], also found Fe had a higher hydrogen conversion than Ni, Co and Cu catalysts. The maximum yield of hydrogen was achieved with the highest carbon deposition in the presence of the Ni-Fe/γ-Al_2O_3 catalyst and had a value of 31.8 mmol $H_2/g_{plastic}$. The higher H_2 yield of the Ni-Fe/γ-Al_2O_3 catalyst among the five catalysts investigated may be associated with the catalyst reduction peak at higher temperatures as shown in Fig. 3, which has been reported to be responsible for hydrogen production [17]. In addition, the small particle size and finely dispersed metal particles (from XRD results) derived from the interaction between metal and γ-

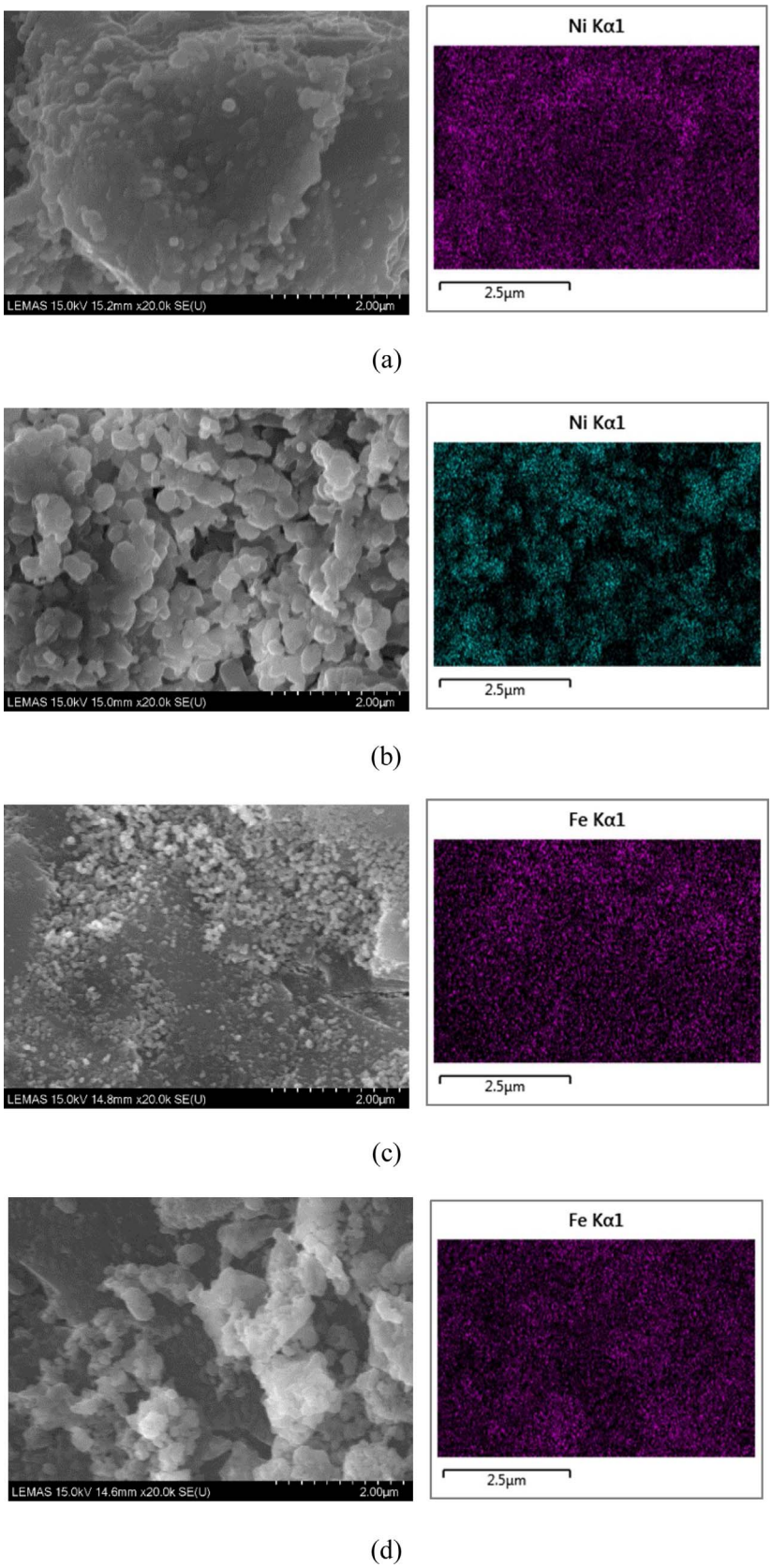

Fig. 4. SEM-EDX results of the fresh catalysts. (a) Ni/γ-Al_2O_3, (b) Ni/α-Al_2O_3, (c) Fe/γ-Al_2O_3, (d) Fe/α-Al_2O_3, (e) Ni-Fe/γ-Al_2O_3, (f) ex-situ reduced Ni-Fe/γ-Al_2O_3.

Al_2O_3 support (TPR analysis), were favorable for hydrogen production from waste plastics. This agreed well with those reports in the literature [40,49] in relation to the catalytic reforming of toluene and ethanol using Ni supported by alumina.

$$C_xH_y \rightarrow C + H_2 \quad (1)$$

Table 1 also shows the gas volumetric content of the product gases. The main gases produced in the absence of catalyst were CH_4, C_2

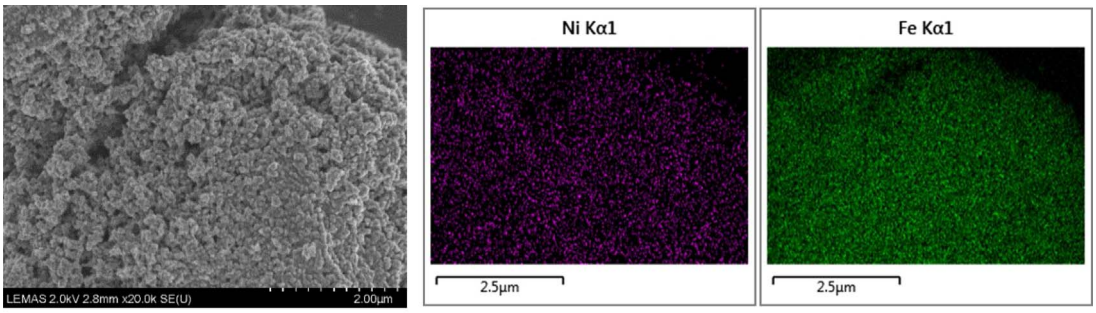

(e)

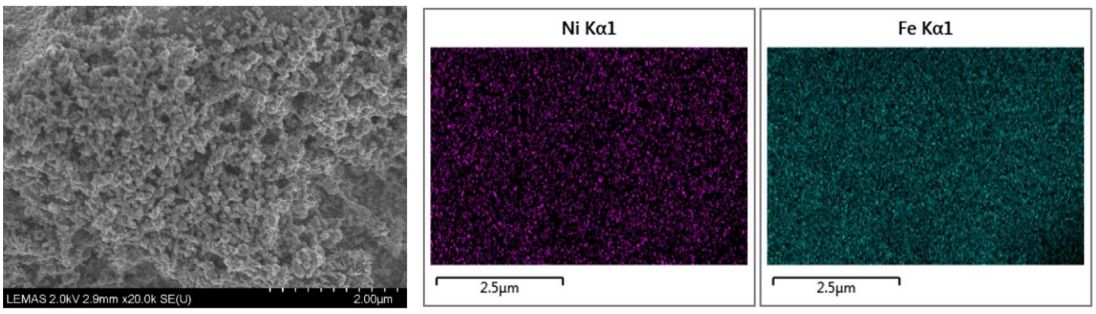

(f)

Fig. 4. (*continued*)

Table 1
Experimental results for the pyrolysis-catalytic process with waste plastics using different catalysts.

	Sand	Ni/γ-Al_2O_3	Ni/α-Al_2O_3	Fe/γ-Al_2O_3	Fe/α-Al_2O_3	Ni-Fe/γ-Al_2O_3
H_2 yield (mmol H_2/$g_{plastic}$)	7.9	22.5	18.0	22.9	20.7	31.8
Gas yield (wt.%)	50.5	41.8	39.6	35.3	32.4	43.0
Liquid (wt.%)	27.8	36.4	37.8	36.2	32.5	19.6
Carbon deposition (wt.%)	2.2	21.1	26.1	32.6	35.2	40.7
Mass balance (%)	80.5	99.2	103.5	104.0	100.1	103.3
Gas composition (vol.%)						
H_2	24.74	52.64	48.43	57.49	57.62	62.88
CO	2.98	4.52	5.45	4.60	4.84	6.24
CH_4	49.36	39.60	41.14	35.81	34.12	27.20
CO_2	0.67	1.39	0.94	0.72	0.64	0.97
C_{2+}	22.25	1.85	4.04	1.38	2.79	2.70

hydrocarbons and H_2. The C_{2+} hydrocarbons comprised more than 20 vol.% of the gases, therefore, cracking reactions were incomplete, which leads to low carbon deposition. For all the catalytic experiments, hydrogen content was greatly increased at the expense of C_{2+} and CH_4 gases. The Ni-Fe/γ-Al_2O_3 catalyst produced the highest H_2 volumetric concentration of 62.88 vol.%, whilst the other monometallic catalysts gave a H_2 content in the range of 48–57 vol.%. Ni (or Fe) supported on γ-Al_2O_3 gave a lower concentration of C_{2+} hydrocarbons than on α-Al_2O_3. In addition, the hydrogen content of the gas product over Fe based catalysts was higher than over Ni based catalysts, again indicating the effective performance of Fe for hydrogen production.

3.1.3. Carbon nanotubes production

Fig. 5 shows the SEM and TEM morphology of the carbon nanomaterials on the surface of the catalyst. The carbon deposits were mainly filamentous type carbon for all the catalysts investigated and were crooked and entangled, with a length of up to tens of microns. A few disordered or amorphous carbons could also be observed. The diameter of the filamentous carbon deposits were variable depending on the catalyst type, generally, deposits on catalysts supported by α-Al_2O_3 appeared to be thicker than those supported by γ-Al_2O_3. The TEM images at high magnifications further demonstrated this difference, and also showed that most of the filamentous carbon nanomaterials on the surface of the catalysts were hollow carbon nanotubes (CNTs). Carbon nanotubes with outer diameters around 20 nm were produced over Ni/γ-Al_2O_3, whereas many disordered deposits were also observed. Compared with Ni/γ-Al_2O_3, the Ni/α-Al_2O_3 catalyst generated thicker carbon nanotubes with diameters ranging from 40 to 50 nm. The difference in morphology may be due to the fact that the metal particle size of the Ni/γ-Al_2O_3 catalyst was smaller than the Ni/α-Al_2O_3 catalyst (from XRD results), since it has been reported that the diameter of carbon nanotubes are dominated by catalyst particle size [34]. In addition, carbon deposits on the Fe/γ-Al_2O_3 catalyst appeared to be smoother and had a smaller diameter than those produced from the α-Al_2O_3 supported Fe/α-Al_2O_3 catalyst. More carbon nanotubes with narrower diameters were observed in the presence of the Ni-Fe/γ-Al_2O_3 catalyst, where the diameters were found to be in the range of 20–40 nm. Therefore, the metal particles available for the carbon growth on the Ni-Fe/γ-Al_2O_3 catalyst were widely distributed and coupled with smaller particle size. This also agrees with the XRD data reported earlier and supports the contention that the enhanced interaction between metal and support promote well distributed, active sites on the surface of the catalyst, resulting in the formation of thinner carbon nanotubes.

In order to better explore the relative amounts of different carbon types on the catalysts, temperature programmed oxidation (TPO) of the reacted catalysts was carried out, and the results are shown in Fig. 6. The small increase in the weight loss from the catalyst at temperatures between 400–500 °C was due to the oxidation of metallic Ni or Fe. According to the weight loss ratio of catalysts after oxidation, Ni based catalysts showed the least carbon deposits, followed by Fe based catalysts. The Ni-Fe/γ-Al_2O_3 catalyst showed the largest weight loss during oxidation, suggesting the largest amount of carbon deposits on the surface of the catalyst. The TPO data are consistent with results from

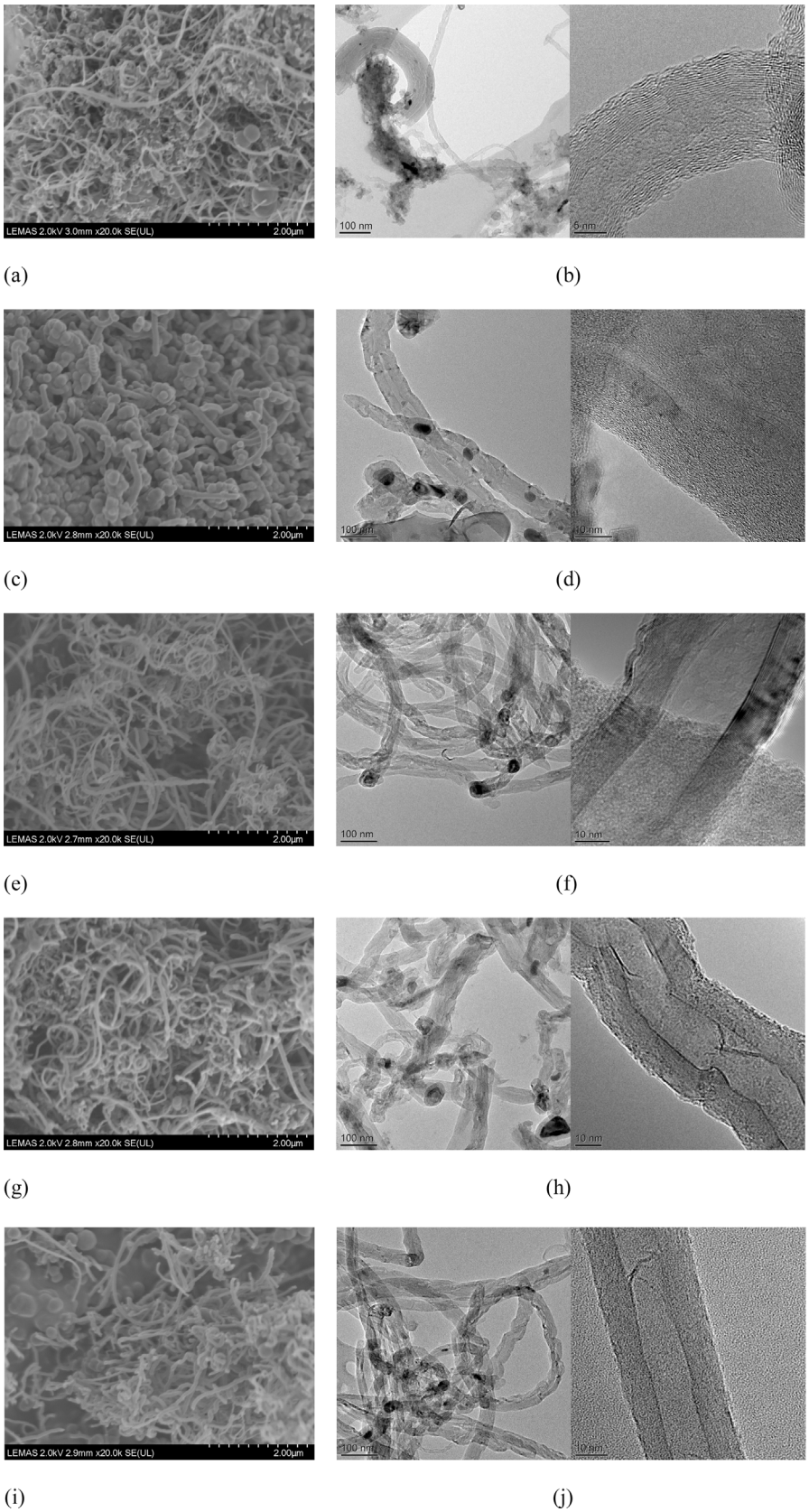

Fig. 5. SEM and TEM images of carbon depositions over (a and b) Ni/γ-Al_2O_3, (c and d) Ni/α-Al_2O_3, (e and f) Fe/γ-Al_2O_3, (g and h) Fe/α-Al_2O_3, (i and j) Ni-Fe/γ-Al_2O_3.

Table 1. The derivative weight loss results of the Ni/γ-Al_2O_3 and Ni/α-Al_2O_3 catalysts gave two distinct peaks at temperatures around 625 and 680 °C. It is reported that the oxidation peak at lower temperature is associated with amorphous carbons, while the peak at higher oxidation temperature is linked to filamentous carbons such as carbon nanotubes, due to them being more stable and less reactive [50]. The amount of each carbon type determined by derivative TPO weight loss data and total deposition yield (Table 1) was calculated and shown in Fig. 6(c).

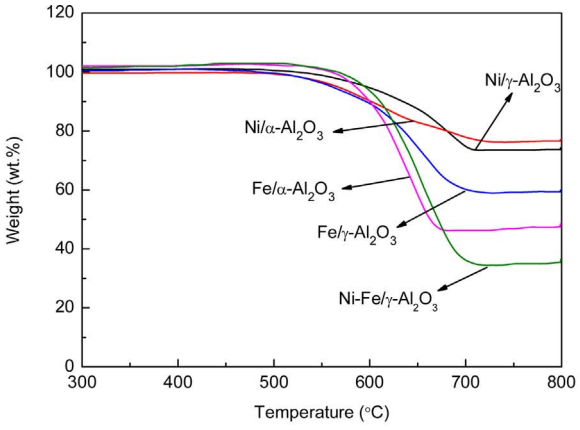

(a)

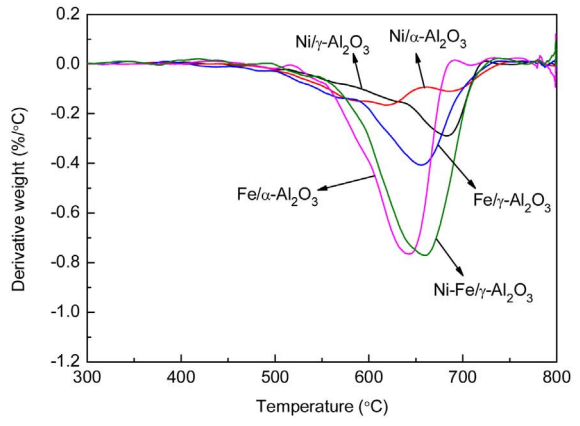

(b)

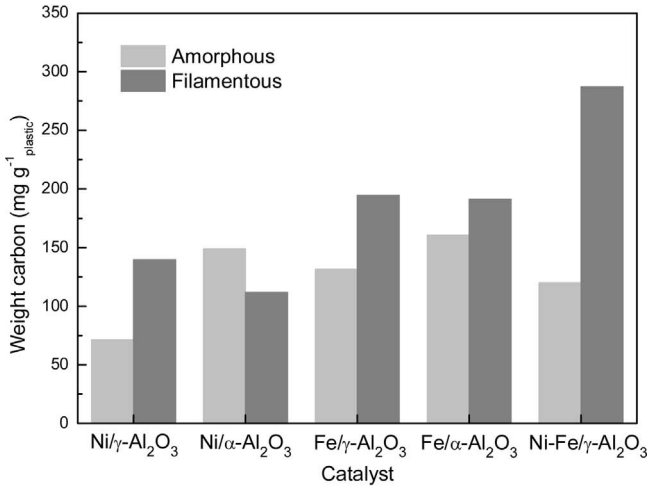

(c)

Fig. 6. (a) Temperature programmed oxidation, (b) derivative plots, (c) amount of different types of carbons over different reacted catalysts.

The Ni/γ-Al_2O_3 catalyst generated a total deposited carbon mass of 211 mg $g_{plastic}^{-1}$, with 71 mg $g_{plastic}^{-1}$ of amorphous type carbons and 140 mg $g_{plastic}^{-1}$ of filamentous carbons. The use of the Ni/α-Al_2O_3 catalyst resulted in a decrease in filamentous carbon deposits, though the total carbons (261 mg $g_{plastic}^{-1}$) was higher than for the Ni/γ-Al_2O_3 catalyst. Since the filamentous carbons deposited on these catalysts, observed from TEM data, were identified as CNTs, the results suggest that Ni/γ-Al_2O_3 produced more CNTs than Ni/α-Al_2O_3. From Fig. 6(b), the oxidation of Fe based catalysts did not present two peaks but a broad large peak. It may consist of two overlapping peaks, while the peak at lower temperature was shifted to higher temperature due to bulk diffusion. The Fe/γ-Al_2O_3 catalyst gave a derivative weight loss peak at higher oxidation temperature, suggesting more filamentous carbons (CNTs) than Fe/α-Al_2O_3. In addition, both Fe/γ-Al_2O_3 and Fe/α-Al_2O_3 catalysts produced more carbon that the Ni-based catalysts probably due to the better carbon solubility of iron compared to nickel [24]. The bimetallic Ni-Fe/γ-Al_2O_3 catalyst showed from Fig. 6(c) that the amount of filamentous carbon with Ni-Fe/γ-Al_2O_3 (287 mg $g_{plastic}^{-1}$) was significantly larger than that obtained for the other catalysts, coupled with a reduction in amorphous carbon deposits (120 mg $g_{plastic}^{-1}$). This suggests that the Ni-Fe/γ-Al_2O_3 catalyst favoured the production of filamentous carbons and reduced the formation of amorphous carbons.

It has been proposed that the growth of carbon nanotubes undergoes three steps: the decomposition of carbon precursors, the diffusion of carbon intermediates on the metal particles, and carbon nucleation and growth to form nanotubes [51]; carbon diffusion was considered to be the rate-controlling step. Yang et al. [13] suggested that smaller metal particles on the catalyst promoted carbon atom diffusion to the metal particle and growth of nanotubes at the interface, leading to a higher CNTs yield. This may explain the observations here, where the catalyst with smaller particle size (from XRD and TEM analysis) generated higher yields of CNTs (from TPO). In addition, α-Al_2O_3 supported Ni (or Fe) catalysts generated more carbon deposition (Table 1), and the obtained specified CNTs yield was lower than from the γ-Al_2O_3 supported catalysts. The data agrees well with the report by Amama et al. [52] in that the yield and quality of carbon nanotubes could be maximized by the increasing porosity of the alumina support.

The carbon nanotubes deposited on the surface of the catalyst from TEM results were found to be not evenly distributed, and some defects in CNTs were also observed. In order to determine the purity and graphitization of the carbon nanotubes, Raman analysis was performed (Fig. 7). The D band around wavelength of 1350 cm^{-1} is ascribed to amorphous or disordered carbon, while the G band at around wavelength 1580 cm^{-1} is caused by tangential vibration of the ordered graphite carbon atoms [53]. The G' band observed at around wavelength 2700 cm^{-1} is associated with the process of two-photon elastic scattering. The peak intensity ratio of I_D/I_G is used to determine the defects and degree of graphitization of carbon deposits, and a higher ratio of $I_{G'}/I_G$ also implies higher carbon nanotubes purity [24,54]. Both Ni/γ-Al_2O_3 and Ni/α-Al_2O_3 catalysts gave an I_D/I_G ratio of about 0.95 and an $I_{G'}/I_G$ ratio of less than 0.4, indicating the poor quality of deposited carbons over the Ni catalysts. The I_D/I_G ratio of the Fe based catalysts was lower than that observed for the nickel counterparts, and

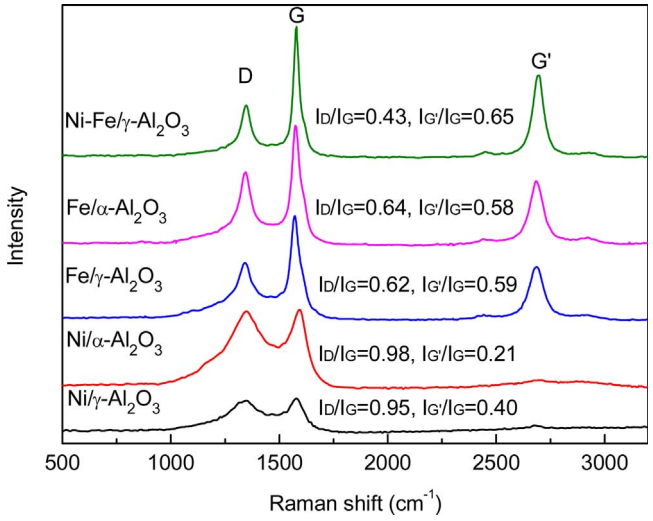

Fig. 7. Raman spectra of the carbon materials over different catalysts.

the $I_{G'}/I_G$ ratio was much higher with a ratio around 0.58. The data is consistent with the morphology observations from Fig. 5 and the amount of filamentous carbons identified from Fig. 6(c). It appears that carbon nanotubes with higher purity and graphitization were more favoured in the presence of Fe catalysts than the Ni catalysts. In addition, although the catalysts using different supports, such as Ni/γ-Al_2O_3 and Ni/α-Al_2O_3 result in a difference in carbon quality, the type of metal in the catalyst has a more significant effect. It implies that it is the metal composition rather than the catalyst support that plays a more important role in relation to the quality of the carbon deposits. From Fig. 7, the minimum I_D/I_G ratio of 0.43 and the maximum of $I_{G'}/I_G$ ratio of 0.65 in the presence of Ni-Fe/γ-Al_2O_3 indicate that the carbon nanotubes obtained had fewer defects and higher graphitic characteristics compared with carbons produced with the other catalysts.

3.2. Hydrogen and carbon nanotubes production with Ni-Fe catalyst

3.2.1. Product yields and gas composition

The Ni-Fe/γ-Al_2O_3 catalyst produced the highest yield of hydrogen and filamentous/CNT, therefore, further work was carried out to investigate the influence of various process parameters on H_2 and CNTs yields using the Ni-Fe/γ-Al_2O_3 catalyst. Results for the product yield and gas production from the catalytic pyrolysis of waste plastics at different process conditions in the presence of the Ni-Fe/γ-Al_2O_3 catalyst are shown in Table 2. Hydrogen yield was increased significantly, from 31.8 mmol $H_2/g_{plastic}$ in the absence of steam to 92.7 mmol $H_2/g_{plastic}$ when the steam to plastic ratio was 2.6. All of the product yield was calculated in relation to the plastic mass only. It can be seen that the increase in the steam injection rate sees a positive effect on the gas production, and gas yield increases to 164.4 wt.% at the steam to plastic ratio of 2.6. Correspondingly, the carbon deposition yield was decreased dramatically from 40.7 to 3.5 wt.%. The carbon reduction is associated with the steam reforming reactions (Eq. (2) and (3)), where hydrocarbons and solid carbons were oxidised by steam and generated more hydrogen and carbon monoxide. The water gas shift reaction Eq. (4) was also enhanced at higher steam feeding rate. This is also in agreement with a number of studies that reported the introduction of steam resulted in a reduction in carbon deposition and an increase in gas yield [18,19]. Liquid yield was also increased because of the introduction of steam into the system.

$$C_xH_y + H_2O \rightarrow CO + H_2 \quad (2)$$

$$C + H_2O \rightarrow CO + H_2 \quad (3)$$

$$CO + H_2O \rightarrow CO_2 + H_2 \quad (4)$$

H_2 production achieved a maximum of 92.7 mmol $H_2/g_{plastic}$ with a H_2 gas concentration of 62.92 vol.% at the steam to plastic ratio of 2.6.

Table 2
Experiment results for pyrolysis-catalytic process of wasted plastics with Ni-Fe/γ-Al_2O_3 at different operation conditions.

	Process Conditions					
Steam to plastic ratio	0	0.3	1	2.6	0	0
Catalyst Temperature, °C	800	800	800	800	700	900
H_2 yield (mmol $H_2/g_{plastic}$)	31.8	34.5	64.4	92.7	27.2	43.7
Gas yield (wt.%)	43	47.7	102.1	164.4	34.1	41.6
Liquid (wt.%)	19.6	59	65.6	120.1	23.8	16.8
Carbon deposition (wt.%)	40.7	31	6.8	3.5	43.2	44
Mass balance (%)	103.3	109	96.8	95.9	101.1	102.4
Gas composition (vol.%)						
H_2	62.88	64.95	64.28	62.92	66.48	72.18
CO	6.24	12.61	24.35	28.05	5.21	5.97
CH_4	27.2	19.12	10.15	6.56	21.43	20.8
CO_2	0.97	0.87	0.71	1.57	1.13	0.81
C_{2+}	2.7	2.45	0.5	0.91	5.74	0.23

The gas compositions at different steam to plastic ratios show (Table 2) that the product gases consist of H_2, CO, CH_4 and a lower content of CO_2 and hydrocarbons. The hydrogen concentration remained stable in the range of 62–65 vol.%. CO content was increased markedly, while CH_4 decreased with increased addition of steam, due to the enhanced reactions Eqs. (2)–(4).

The product distributions and gas composition from waste plastics at different catalyst temperatures in the absence of steam are also shown in Table 2. The results show that the hydrogen yield increased from 27.2 to 43.7 mmol $H_2/g_{plastic}$ when the catalyst temperature was increased from 700 to 900 °C, while carbon deposition on the catalyst remained high and in the range of 40–44 wt.%. The lowest gas yield of 34.1 wt.% corresponded with the highest liquid yield of 23.8 wt.% obtained at 700 °C. In addition, from the gas composition the C_{2+} hydrocarbon content (5.74 vol.%) of the product gas was higher at 700 °C than at 800 and 900 °C. It is suggested that the thermal cracking at low temperature is relatively weak, and some hydrocarbons cannot be completely converted, leading to a lower gas production but a higher yield of condensed liquid. When the catalyst temperature was raised from 800 to 900 °C, hydrogen yield was significantly increased to 87.39 mg $g_{plastic}^{-1}$ and H_2 gas concentration also increased to 72.18 vol.%, at the expense of the consumption in CH_4 and C_{2+} gases.

3.2.2. Effect of steam on carbon nanotubes production

Fig. 8. shows the scanning electron microscopy determined morphological appearance of the reacted Ni-Fe/γ-Al_2O_3 catalysts at different steam to plastic ratios. Carbon deposits on the catalyst in the absence of steam were predominantly filamentous carbons with a dense covering on the surface of the Ni-Fe/γ-Al_2O_3 catalyst. At the steam to plastic ratio of 0.3 and 1, the nature of the deposited carbons appeared to be quite similar, and both filamentous carbon and amorphous deposits were observed. The diameter of these filament-like carbons was stable, irrespective of the different steam injection rates used. However, when the ratio of steam to plastic was increased to 2.6, almost no filamentous carbon deposits could be observed. It appears that almost all of the carbon deposits reacted with the increased steam. This agrees well with the experimental results shown in Table 2 that reports very low levels of carbon deposits at the highest steam to plastic ratio.

The decrease in the amount of carbon deposition with more steam injection can be further demonstrated by the TPO analysis, shown in Fig. 9(a) and the derivative weight loss in Fig. 9(b). The low carbon content of the used catalyst at the steam to plastic ratio of 2.6 is confirmed by the TPO data shown in Fig. 9. As the steam to plastic ratio was increased from 0 to 1, the thermal stability of the carbon deposits was decreased as the temperature of the main oxidation peak shifted to a lower temperature. From Fig. 9(c), as the steam to plastic ratio was raised, the amount of filamentous carbons decreased, producing 287 mg $g_{plastic}^{-1}$ without steam injection, compared with 130 and 17 mg $g_{plastic}^{-1}$ at ratios of 0.3 and 1, respectively. The amount of amorphous carbons obtained showed a maximum at the steam to plastic ratio of 1. Both amorphous and filamentous carbons were gasified when the steam to plastic ratio increased from 0.3 to 1.

Raman spectra was also used to characterise the deposited carbons at different steam to plastic ratios (Fig. 10). It can be seen that the intensity of the G and G' peaks of the carbons were strong at 0 and 0.3 steam to plastic ratios, indicating a graphitic nature of the deposited carbons. However, the I_D/I_G ratio was increased from 0.43 to 0.75 and further reached to 0.92, when the steam to plastic ratio was raised from 0 to 1. The data suggesting a large decrease in the quality and purity of ordered carbon nanotubes with the introduction of steam. This agreed well with results from Fig. 9(c) which showed that most filamentous carbon were consumed at higher steam inputs, leading to poor carbon quality.

3.2.3. Effect of catalyst temperature on carbon nanotubes production

The TEM images of the carbon deposits over the Ni-Fe/γ-Al_2O_3

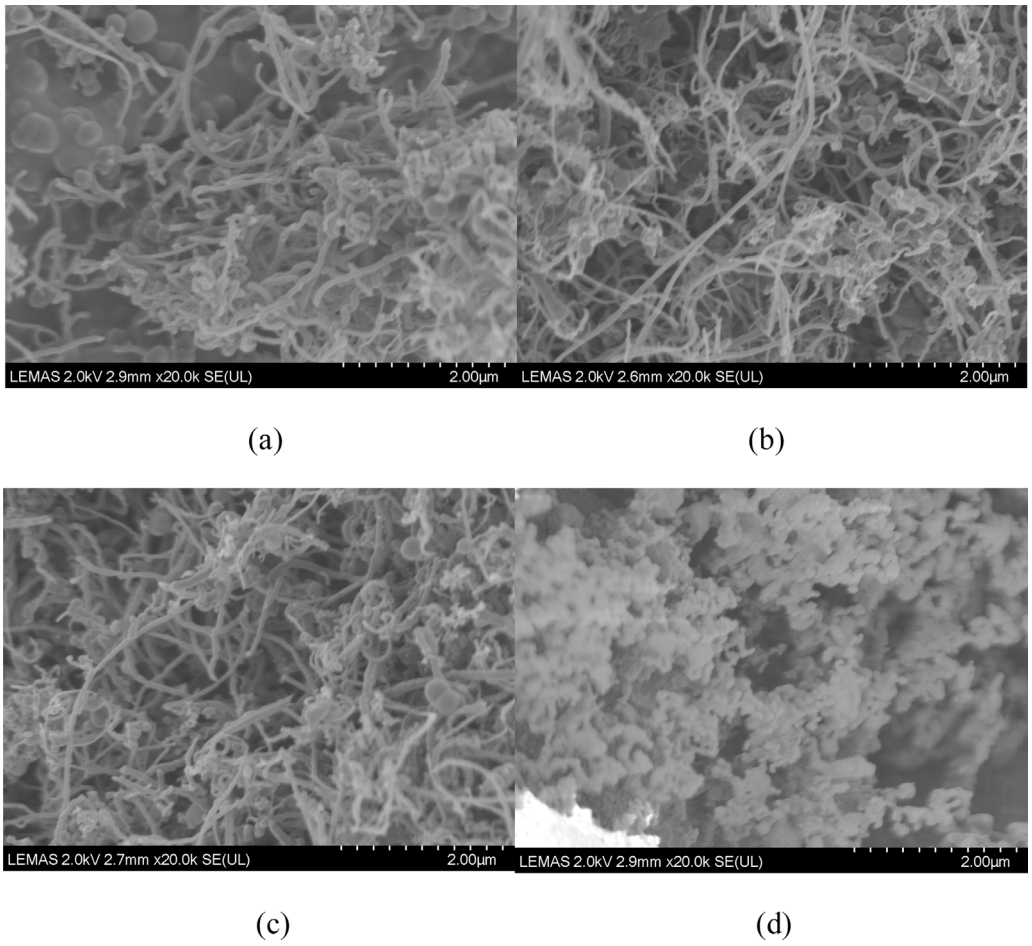

Fig. 8. SEM images of spent Ni-Fe/γ-Al_2O_3 with different steam to plastic ratios. (a) 0, (b) 0.3, (c) 1, (d) 2.6.

catalyst at different catalyst temperatures are shown in Fig. 11. The TEM micrographs show the presence of bamboo-like, straight, as well as crooked filamentous carbon nanotubes produced at the catalyst temperature of 700 °C, with diameters ranging from 20 to 40 nm and length up to several microns. Multiwalled carbon nanotubes could also be found on the catalyst used at 800 °C catalyst temperature with similar lengths but more even distribution of diameters and shapes compared with 700 °C catalyst temperature. Moreover, the open tips or the hollow tip observed from the TEM images implies the base-growth model of the CNTs growth [55]. Encapsulating carbons with large metal particle size were found on the catalyst used at 900 °C (Fig. 11(c)), and carbon nanofibers without hollow structures were also produced on the catalyst. The formation of various types of carbon (including amorphous carbon, carbon nanotubes and nanofibers) may be due to aggregation of the catalyst particles at high catalyst temperature, as the increase in metal particle size was reported to favour the nonselective forms of carbon [56,57].

The type and relative amount of carbon nanomaterials were examined by TPO analysis. The oxidative weight loss of the used catalysts is shown in Fig. 12(a) and shows the large amounts of catalyst carbon deposits produced at all catalyst temperatures. The maximum temperature of weight loss shown from the derivate peak was shifted to a higher oxidation temperature when the catalyst temperature was increased to 900 °C, indicating high carbon growth temperatures were likely to produce less amorphous carbons. Fig. 12(c) shows that the amount of filamentous carbon generated from waste plastics increased from 258 to 360 mg $g_{plastic}^{-1}$ when the catalyst temperature was raised from 700 to 900 °C. This is in accordance with previous work with a different feedstock (tyres) that likewise found that high catalyst temperature promoted the production of filamentous carbons [19]. The amount of amorphous carbon deposited over the Ni-Fe/γ-Al_2O_3 catalyst was significantly higher at 700 °C, at 174 mg g^{-1} plastic, than at the catalyst temperatures of 800 and 900 °C with yields of 120 and 80 mg g^{-1} plastic respectively. This indicates that the high catalyst temperature favoured the production of filamentous carbons and restricted the amount of amorphous carbon produced.

Raman spectroscopy was also carried out for carbon deposits in relation to different catalyst temperatures for the pyrolysis-catalysis of the waste plastics. From Fig. 13, the peaks of D, G as well as G' can be observed, with the relative intensity of these peaks varying with the catalyst temperature. The results showed that the D peak decreased while the G peak increased when the catalyst temperature was increased from 700 to 800 °C, indicating more carbon nanotubes with higher purity and graphitic nature were formed at a catalyst temperature of 800 °C. However, there was a reduction in the quality of carbons deposited on the catalyst at 900 °C, with an I_D/I_G ratio of 0.75 which was higher than the carbons produced at a catalyst temperature of 800 °C. This correlated with the structure defects in the carbon which were observed from Fig. 11(d) where some disordered and uneven graphitic layers of carbons at 900 °C were formed. Carbon nanofibers have been reported to give a broad Raman spectra compared to nanotubes [58], thus the weaker Raman peak of the carbon produced at the catalyst temperature of 900 °C in Fig. 13 further suggests the presence of carbon nanofibers. It also implies that it is incorrect to determine the quality of carbon deposits based only on temperature programmed oxidation analysis and/or electron microscopy, multiple technologies in terms of structure, defects, oxidation behaviour and amount should be combined to value the properties of the product carbon.

The TPO results reveal that more of the waste plastics were converted into filamentous carbon as the catalytic temperature was

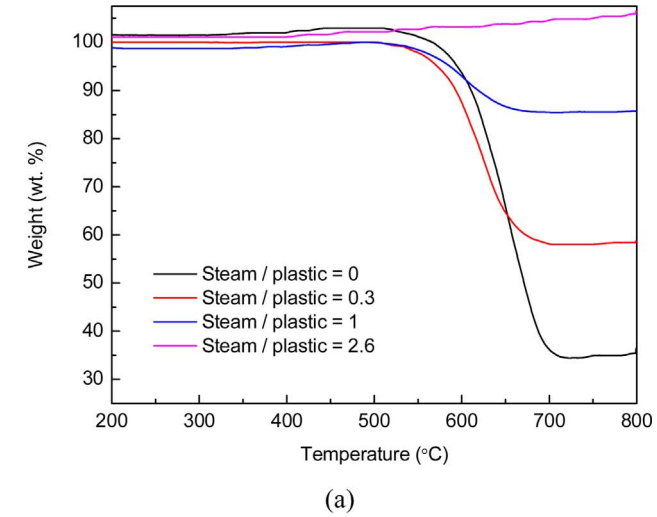

(a)

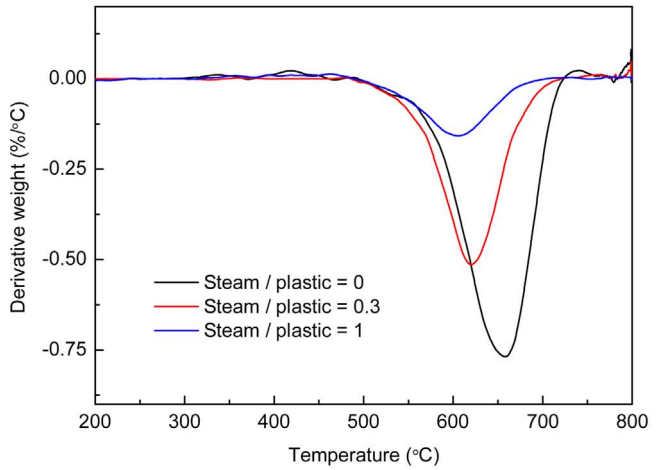

(b)

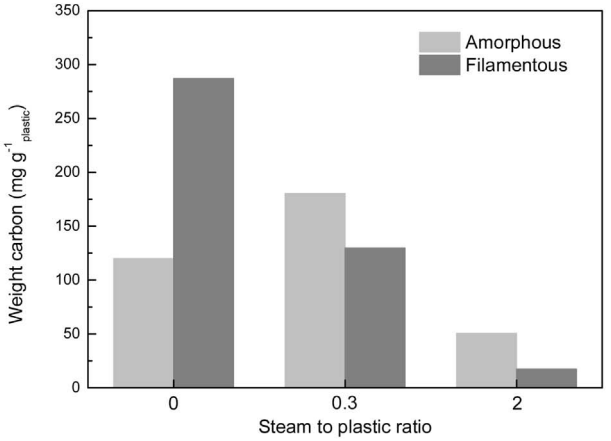

(c)

Fig. 9. (a) Temperature programmed oxidation, (b) derivative plots, (c) amount of different types of carbonson spent Ni-Fe/γ-Al_2O_3 with different steam to plastic ratios.

increased. In addition, Raman analysis shows that the quality of the carbon increased from 700 to 800 °C, but decreased at 900 °C. TEM characterisation of the catalyst found that at temperatures of 700 and 800 °C, filamentous carbons are more likely to be in the form of CNTs.

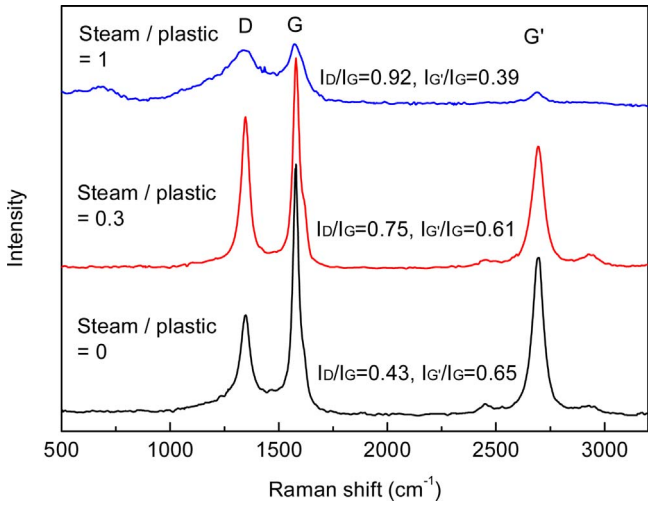

Fig. 10. Raman spectra of the carbon materials at different steam to plastic ratios.

The growth efficiency of CNTs has been reported to be related to the carbon feeding rate, and the continuous growth of CNTs can only be achieved at their matched feeding rate [59]. As the temperature influences the decomposition rate of the plastic feedstock and thereby the amount of carbon precursors fed to the catalyst, it implies that in this work, 800 °C generated a more suitable carbon source for CNTs growth than at the lower temperature of 700 °C. However, further increase in temperature (900 °C) provided an excessive feeding of carbon via increased supply of pyrolysis gases, which caused the metal particles to be poisoned. In addition, the agglomeration of metal particles at high temperature resulted in large catalyst particles and filamentous carbon with large diameters, or even carbon nanofibers as demonstrated by TEM.

4. Conclusions

Product yields, including gas, liquid, deposited carbon and hydrogen as well as the quality of carbon nanotubes (CNTs) were significantly influenced by the catalyst composition. In terms of catalyst support material, the α-Al_2O_3 supported catalyst had weaker interaction between metal and support than γ-Al_2O_3, leading to a higher yield, but lower quality of carbon CNTs deposits. CNTs with higher purity and graphitization were more favoured in the presence of Fe catalysts than Ni. In addition, Fe based catalysts generated higher yields of hydrogen and CNTs than Ni catalysts, due to the higher cracking activity of hydrocarbon cracking reactions. Bimetallic Ni-Fe catalyst could be considered as a desirable catalyst for pyrolysis of waste plastics producing both hydrogen and CNTs in significant quantities. The suitable interaction between metal oxides and alumina support resulted in finely dispersed catalyst particles, which benefited both the growth of carbon nanotubes and the hydrogen production.

For the Ni-Fe/γ-Al_2O_3 catalyst, hydrogen yield was greatly increased from 31.8 to 92.7 mmol $H_2/g_{plastic}$ when the steam to plastic ratio was raised from 0 to 2.6, whereas carbon deposits decreased rapidly to 3.5 wt.%. Higher catalyst temperature favoured both the hydrogen and filamentous carbon production. However, further increase in temperature (to 900 °C) led to non-selective types of carbon with lower quality, due to the agglomeration of catalyst particles. A maximum CNTs yield of 287 mg $g_{plastic}^{-1}$ and hydrogen yield of 31.8 mmol $H_2/g_{plastic}$ were obtained over the Ni-Fe/γ-Al_2O_3catalyst at 800 °C without steam addition.

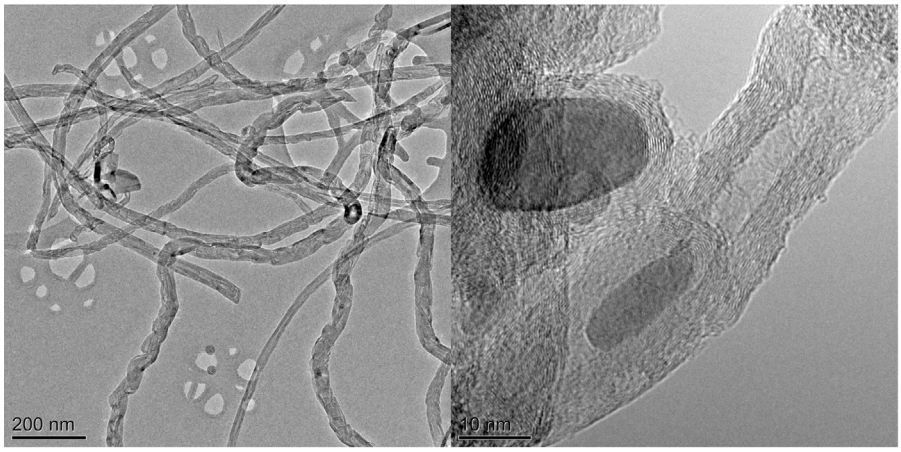

(a)

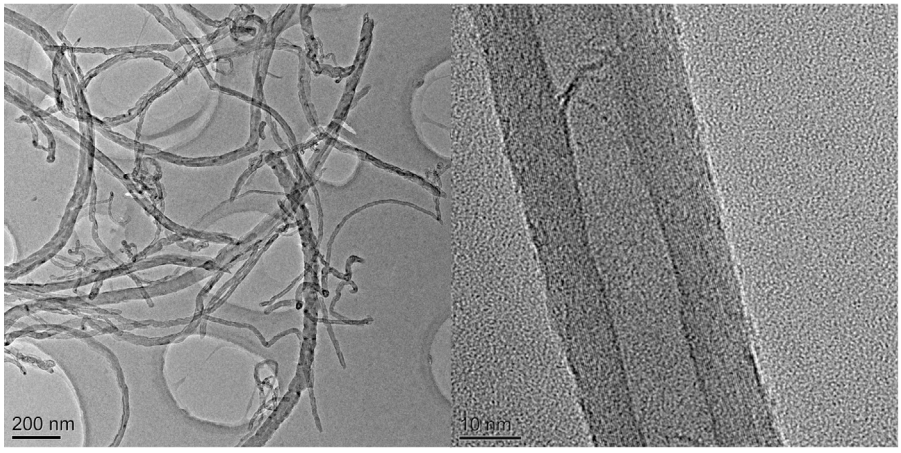

(b)

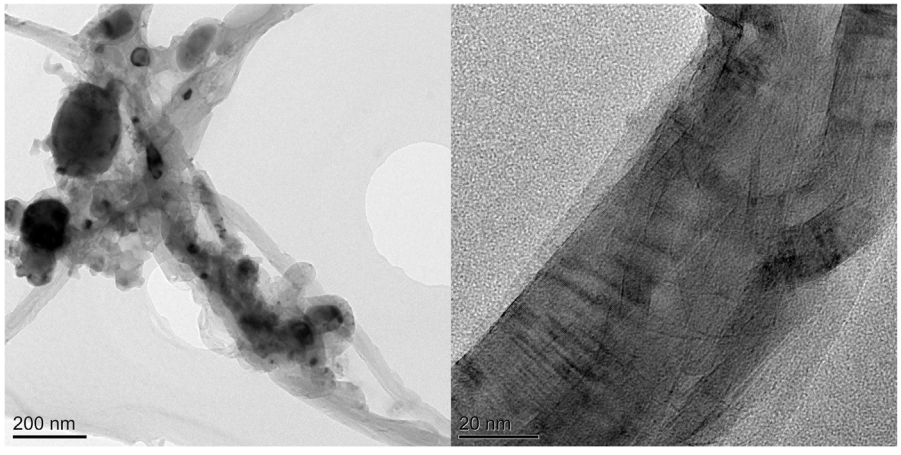

(c)

Fig. 11. TEM images of spent Ni-Fe/γ-Al_2O_3 with different catalyst temperatures. (a) 700, (b) 800, (c) 900 °C.

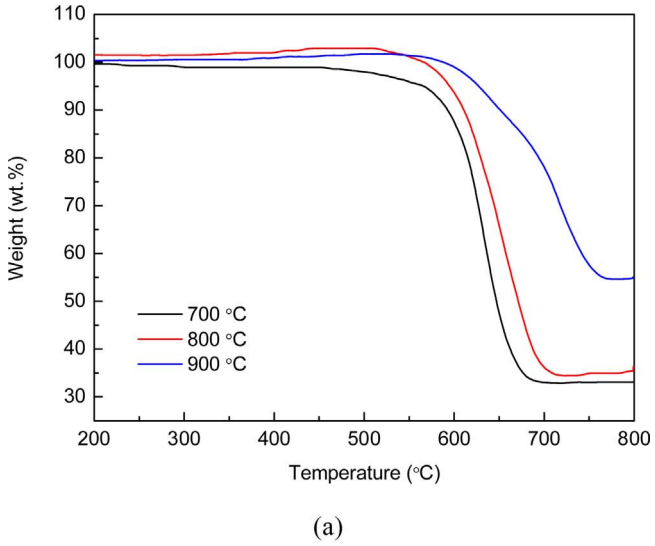

(a)

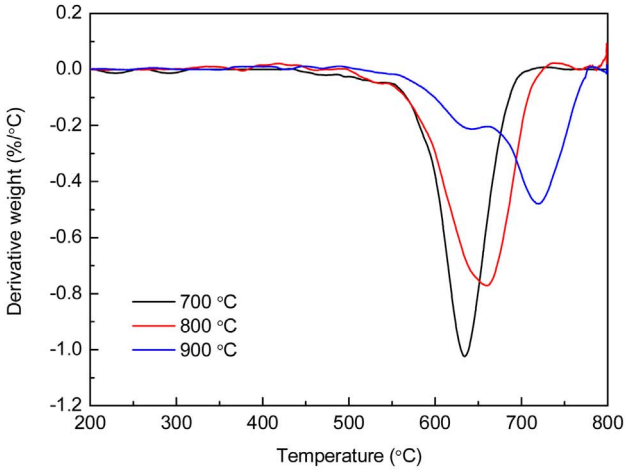

(b)

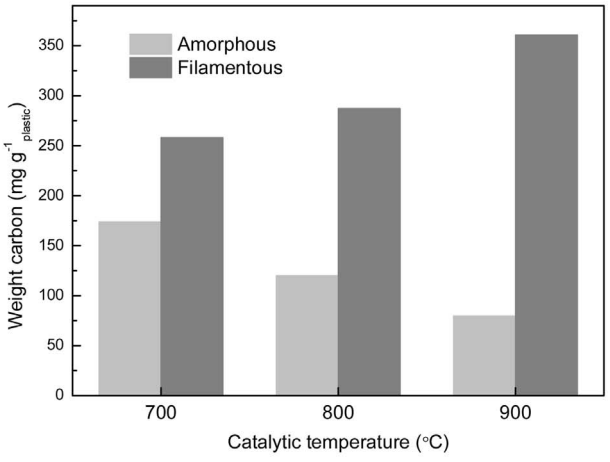

(c)

Fig. 12. (a) Temperature programmed oxidation, (b) derivative plots, (c) amount of different types of carbonson spent Ni-Fe/γ-Al_2O_3 at different catalytic temperatures.

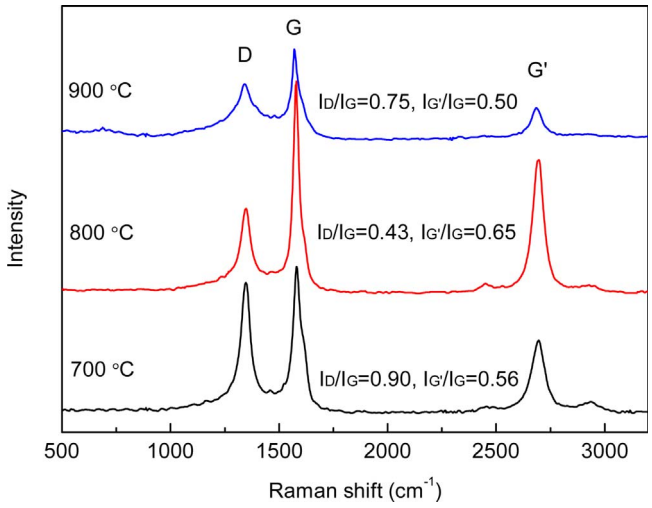

Fig. 13. Raman spectra of the carbon materials over different catalysts.

Acknowledgements

The authors wish to express their sincere thanks for the financial support from the National Natural Science Foundation of China (51622604), the China Postdoctoral Science Foundation (2016M602293) and the Foundation of State Key Laboratory of Coal Combustion (FSKLCCB1610). The experiment was also assisted by the Analytical and Testing Center in Huazhong University of Science & Technology (http://atc.hust.edu.cn, Wuhan 430074 China), and the Analysis Laboratory in the School of Chemical and Process Engineering at the University of Leeds. This project has received funding from the European Union's Horizon 2020 research and innovation programme under the Marie Sklodowski-Curie grant agreement No. 643322 (FLEXI-PYROCAT).

References

[1] B. Kunwar, H. Cheng, S.R. Chandrashekaran, B.K. Sharma, Renew. Sust. Energy Rev. 54 (2016) 421–428.
[2] S. Al-Salem, A. Antelava, A. Constantinou, G. Manos, A. Dutta, J. Environ. Manage. 197 (2017) 177–198.
[3] F.J. Passamonti, U. Sedran, Appl Catal. B: Environ. 125 (2012) 499–506.
[4] C. Wu, M.A. Nahil, N. Miskolczi, J. Huang, P.T. Williams, Environ. Sci. Technol. 48 (2013) 819–826.
[5] J.C. Acomb, C. Wu, P.T. Williams, J. Anal Appl. Pyrol. 113 (2015) 231–238.
[6] C. Wu, M.A. Nahil, N. Miskolczi, J. Huang, P.T. Williams, Process Saf. Environ. Part A 103 (2016) 107–114.
[7] S. Iijima, Nature 354 (1991) 56.
[8] S. Kumar, R. Rani, N. Dilbaghi, K. Tankeshwar, K.-H. Kim, Chem. Soc. Rev. 46 (2017) 158–196.
[9] M.F. De Volder, S.H. Tawfick, R.H. Baughman, A.J. Hart, Science 339 (2013) 535–539.
[10] K.A. Shah, B.A. Tali, Mater. Sci. Semicon. Proc. 41 (2016) 67–82.
[11] G. Wang, H. Wang, Z. Tang, W. Li, J. Bai, Appl. Catal. B: Environ. 88 (2009) 142–151.
[12] J. Liu, Z. Jiang, H. Yu, T. Tang, Polym. Degrad. Stabil. 96 (2011) 1711–1719.
[13] R.-X. Yang, K.-H. Chuang, M.-Y. Wey, Energy Fuel (2015).
[14] Q. Weizhong, L. Tang, W. Zhanwen, W. Fei, L. Zhifei, L. Guohua, L. Yongdan, Appl. Catal. A: Gen. 260 (2004) 223–228.
[15] Y. Shen, A.C. Lua, Appl. Catal. B: Environ. 164 (2015) 61–69.
[16] C. Wu, P.T. Williams, Int. J. Hydrogen Energy 35 (2010) 949–957.
[17] M.A. Nahil, C. Wu, P.T. Williams, Fuel Process. Technol. 130 (2015) 46–53.
[18] J.C. Acomb, C. Wu, P.T. Williams, Appl. Catal. B: Environ. 147 (2014) 571–584.
[19] Y. Zhang, P.T. Williams, J. Anal Appl. Pyrol. 122 (2016) 490–501.
[20] K. Hernadi, A. Fonseca, J.B. Nagy, A. Siska, I. Kiricsi, Appl. Catal. A: Gen. 199 (2000) 245–255.
[21] J. Gong, J. Liu, Z. Jiang, J. Feng, X. Chen, L. Wang, E. Mijowska, X. Wen, T. Tang, Appl. Catal. B: Environ. 147 (2014) 592–601.
[22] M. Chhowalla, K. Teo, C. Ducati, N. Rupesinghe, G. Amaratunga, A. Ferrari, D. Roy, J. Robertson, W. Milne, J. Appl. Phys. 90 (2001) 5308–5317.
[23] X. Wen, X. Chen, N. Tian, J. Gong, J. Liu, M.H. Rümmeli, P.K. Chu, E. Mijiwska, T. Tang, Environ. Sci. Technol. 48 (2014) 4048–4055.
[24] J.C. Acomb, C. Wu, P.T. Williams, Appl. Catal. B: Environ. 180 (2016) 497–510.
[25] A.C. Lua, H.Y. Wang, Appl. Catal. B: Environ. 156 (2014) 84–93.
[26] R. Cartwright, S. Esconjauregui, D. Hardeman, S. Bhardwaj, R. Weatherup, Y. Guo, L. D', Arsié, B. Bayer, P. Kidambi, S. Hofmann, E. Wright, J. Clarke, D. Oakes, C. Cepek, J. Robertson, Carbon 81 (2015) 639–649.
[27] C. Wu, P.T. Williams, Appl. Catal. B: Environ. 96 (2010) 198–207.
[28] C. Wu, P.T. Williams, Appl. Catal. B: Environ. 87 (2009) 152–161.

[29] B. Kaya, S. Irmak, A. Hasanoğlu, O. Erbatur, Int. J. Hydrogen Energy 40 (2015) 3849–3858.
[30] Y. Shen, P. Zhao, Q. Shao, F. Takahashi, K. Yoshikawa, Appl. Energy 160 (2015) 808–819.
[31] W. Shen, F.E. Huggins, N. Shah, G. Jacobs, Y. Wang, X. Shi, G.P. Huffman, Appl. Catal. A: Gen. 351 (2008) 102–110.
[32] C. He, N. Zhao, Y. Han, J. Li, C. Shi, X. Du, Mater. Sci Eng. A: Struct. 441 (2006) 266–270.
[33] C.L. Cheung, A. Kurtz, H. Park, C.M. Lieber, J. Phys. Chem. B 106 (2002) 2429–2433.
[34] D. Chen, K.O. Christensen, E. Ochoa-Fernández, Z. Yu, B. Tøtdal, N. Latorre, A. Monzón, A. Holmen, J. Catal. 229 (2005) 82–96.
[35] S. Takenaka, M. Ishida, M. Serizawa, E. Tanabe, K. Otsuka, J. Phys. Chem. B 108 (2004) 11464–11472.
[36] M.A. Ermakova, D.Y. Ermakov, A.L. Chuvilin, G.G. Kuvshinov, J. Catal. 201 (2001) 183–197.
[37] D. Yao, C. Wu, H. Yang, Y. Zhang, M.A. Nahil, Y. Chen, P.T. Williams, H. Chen, Energy Convers. Manage. 148 (2017) 692–700.
[38] L.G. Briquet, C.R.A. Catlow, S.A. French, J. Phys. Chem. C 112 (2008) 18948–18954.
[39] C. Wu, P.T. Williams, Fuel 89 (2010) 1435–1441.
[40] A.L. Alberton, M.M. Souza, M. Schmal, Catal. Today 123 (2007) 257–264.
[41] Y. Liu, J. Gao, Q. Liu, F. Gu, X. Lu, L. Jia, G. Xu, Z. Zhong, F. Su, RSC Adv. 5 (2015) 7539–7546.
[42] J. Gao, C. Jia, M. Zhang, F. Gu, G. Xu, F. Su, Catal. Sci. Technol. 3 (2013) 2009–2015.
[43] M. Al-Dossary, J. Fierro, Appl. Catal. A: Gen. 499 (2015) 109–117.
[44] Y. Zhang, C. Wu, A. Nahil, P.T. Williams, Energy Fuel 29 (2015) 3328–3334.
[45] P. Bolt, F. Habraken, J. Geus, J. Catal. 151 (1995) 300–306.
[46] L. Garcia, A. Benedicto, E. Romeo, M. Salvador, J. Arauzo, R. Bilbao, Energy Fuel 16 (2002) 1222–1230.
[47] L. Wang, D. Li, M. Koike, S. Koso, Y. Nakagawa, Y. Xu, K. Tomishige, Appl. Catal. A: Gen. 392 (2011) 248–255.
[48] M. Sánchez-Sánchez, R. Navarro, J. Fierro, Int. J. Hydrogen Energy 32 (2007) 1462–1471.
[49] M. Kong, J. Fei, S. Wang, W. Lu, X. Zheng, Bioresour. Technol. 102 (2011) 2004–2008.
[50] W. Li, H. Wang, Z. Ren, G. Wang, J. Bai, Appl. Catal. B: Environ. 84 (2008) 433–439.
[51] A.E. Awadallah, A.A. Aboul-Enein, A.K. Aboul-Gheit, Energy. Convers. Manage. 77 (2014) 143–151.
[52] P.B. Amama, C.L. Pint, S.M. Kim, L. McJilton, K.G. Eyink, E.A. Stach, R.H. Hauge, B. Maruyama, ACS Nano 4 (2010) 895–904.
[53] J. Gong, J. Liu, D. Wan, X. Chen, X. Wen, E. Mijowska, Z. Jiang, Y. Wang, T. Tang, Appl. Catal. A: Gen. 449 (2012) 112–120.
[54] Y. Shen, W. Gong, B. Zheng, L. Gao, Appl. Catal. B: Environ. 181 (2016) 769–778.
[55] M. Pudukudy, Z. Yaakob, M.S. Takriff, Energy Convers. Manage. 126 (2016) 302–315.
[56] M. Perez-Cabero, I. Rodrıguez-Ramos, A. Guerrero-Ruız, J. Catal. 215 (2003) 305–316.
[57] Y.-H. Chung, S. Jou, Mater. Chem. Phys. 92 (2005) 256–259.
[58] N. De Greef, L. Zhang, A. Magrez, L. Forró, J.-P. Locquet, I. Verpoest, J.W. Seo, Diam. Relat. Mater. 51 (2015) 39–48.
[59] C. Lu, J. Liu, J. Phys. Chem. B 110 (2006) 20254–20257.